

Interactive Neural Network Texture Analysis and Visualization for Surface Reconstruction in Medical Imaging

C. Busch, M.H. Groß

Visual Computing Group, Computer Graphics Center, Wilhelminenstraße 7, D 6100 Darmstadt, Germany

Abstract

The following paper describes a new approach for the automatic segmentation and tissue classification of anatomical objects such as brain tumors from magnetic resonance imaging (MRI) data sets using artificial neural networks. These segmentations serve as an input for 3D-reconstruction algorithms. Since MR images require a careful interpretation of the underlying physics and parameters, we first give the reader a tutorial style introduction to the physical basics of MR technology. Secondly, we describe our approach that is based on a two-pass method including non-supervised cluster analysis, dimensionality reduction and visualization of the texture features by means of nonlinear topographic mappings. An additional classification of the MR data set can be obtained using a post-processing technique to approximate the Bayes decision boundaries. Interactions between the user and the network allow an optimization of the results. For fast 3D-reconstructions, we use a modified marching cubes algorithm but our scheme can easily serve as a preprocessor for any kind of volume renderer.

The applications we present in our paper aim at the automatic extraction and fast reconstruction of brain tumors for surgery and therapy planning. We use the neural networks on pathological data sets and show how the method generalizes to physically comparable data sets.

Keywords: Artificial Neural Networks, Cluster Analysis, Texture Analysis, Magnetic Resonance Imaging, Subspace Mapping, Visualization of Multidimensional Feature Spaces, Tissue Classification, 3D-Reconstruction, Marching Cubes, Brain Tumors

1. Introduction

Volumetric rendering has become increasingly important during the last few years, in particular in the field of medical imaging. Advanced volume renderers, as in [10],[13] or [17] have been developed as well as 3D surface reconstruction methods like marching cubes[16] or Delaunay triangulation. However there is still one presumption for all these methods. In order to provide reliable and high-quality images both 3D-reconstruction algorithms and volume renderers require a robust pre-segmentation of the initial 3D data sets to be analyzed. Most methods presented to date, are either based on a linear separation of the grey values[19] or the voxels to be rendered are treated interactively[10].

For a robust segmentation however there are two ways to pre-segment the data material. The first possibility arises when dealing with magnetic resonance imaging, where a multiparameter image can be generated and then be clustered and segmented pixelbased with standard statistical methods as [2],[4] or with Fuzzy approaches as in [8]. In practice however, multiparameter scans are too expensive and too stressful for the patients. Thus, the most promising way to extract features from grey level images are texture analysis techniques describing the local pattern to be discriminated in a texture feature space. In addition to classical methods stemming from image processing[5] adaptive non-linear paradigms, like artificial neural networks[14] have proved to be a promising alternative for many applications. After extracting features from the data, the problem of clustering and classification can be treated with methods of statistical data analysis. The objective of clustering is to find an optimal representation of the data distribution by means of a discrete and limited set of mean vectors or centroids, whereas classification aims at defining minimum error decision boundaries using a statistically representative set of training vec-

tors. There are numerous mathematical methods to solve this problem from C-means clustering to maximum likelihood estimation. But most computationally inexpensive methods assume too many restrictions on the underlying statistical distribution of the data. For this reason, the advantages of neural network feature extraction, clustering and classification have been discovered during the last few years [21].

The following paper describes a discrimination method for magnetic resonance data based on topological mappings of Kohonen[11],[12]. Based on application studies as in [6] and [7] these paradigms have been adapted and extended by the authors. It will be shown that the network performs both feature extraction, clustering and classification in a unique approach. Moreover, because of the topological organization of network's neurons it also performs a nonlinear subspace mapping from the high dimensional texture feature space into the RGB color space and corresponding colors refer to similarities of local texture features in the image. With this capability, the network also provides a visualization method for high dimensional feature spaces and results in an interesting alternative to standard methods, as [1] or [24].

The organization of our paper is as follows: First, for reasons of understanding the underlying physical meaning of MR-images, we give a tutorial-style brief introduction to the principles of magnetic resonance imaging. Then we describe the topology and the training rules of the neural network which we adapted for our purposes and explain the visualization technique we developed. In particular when approaching the Bayes decision boundaries with the network, the user is able to interact with the neurons of the network and to modify class assignments. For a fast 3D surface reconstruction we use a modified marching cubes technique. The application of our method on the extraction, classification and 3D-reconstruction of brain tumors shows its capabilities and illustrates the visualization technique.

2. Physical Foundations of MR-Imaging

2.1. General Remarks

Magnetic resonance imaging is one of the most effective methods so far developed to give an in vivo insight into the human body. Providing 3D volume data sets, MR images have often been used to illustrate the capabilities of rendering and reconstruction techniques. However, in contrast to standard Computer x-ray tomography, where the data set always presents the density of the analyzed volume, MR images are much more complex in the underlying understanding of quantum mechanics. Moreover, the interpretation of MR images strongly depend on the parameter sequences used for the recording process. In order to develop a reliable automatic method for data analysis, it is of crucial importance that the physics of the MR method are understood. The following section will briefly introduce the basic physics using a simplified mechanical model and explain the meaning of the three main parameters that can be measured, namely the longitudinal relaxation time T_1 , the transversal relaxation time T_2 and the proton's density. A good introduction to MR-imaging can be found in [15] or [20].

2.2. Magnetic Resonance and the Lamor Equation

Magnetic resonance is a phenomenon that was discovered in the 40ies. The phenomenon is based on the interaction of atomic nuclei, located in a constant magnetic field, with an electromagnetic high frequency (HF) field. From the point of view of classical physics this interaction can be explained as a precession of the nuclei's spin with an isotope dependent frequency, called Lamor frequency. The precession itself is stimulated by means of the HF field. This is illustrated in figure 1.

Any atomic nucleus that consists of an odd number of protons and neutrons is characterized by an angular momentum or spin. From the point of view of classical physics the spin gives rise to a circular current due to the positive charge of the nucleus, and thus to a magnetic momentum. In this way, the nucleus can be interpreted as a tiny magnet. If we expose it to an external magnetic field the direction of the spin will change according to the external force (see figure 1a). During that relaxation process of the nucleus, the spin will describe a precession movement for a short time with a characteristic frequency, the so-called Lamor frequency ω . According to eq. 1 the Lamor frequency depends on the strength B_0 of the external field and on a constant γ .

$$\omega = \gamma \cdot B_0 \tag{1}$$

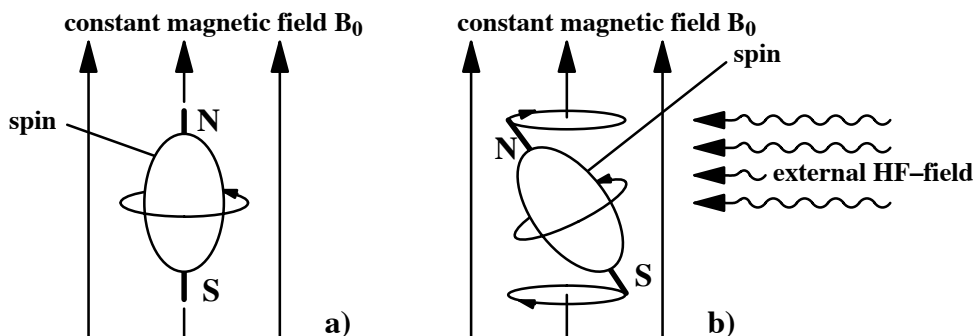


Figure 1. Simplified model for magnetic resonance of a nucleus stimulated by an external HF-field
 a) spin oriented in a constant magnetic field B_0
 b) precession of the spin stimulated by a transient HF-impulse

After being oriented towards the direction of this external field, the nucleus' relaxation can be stimulated again by additional transient HF impulses. In order to achieve resonance and in-phase precession, the frequency of the transient field has to correspond to the Larmor frequency of the nucleus.

In most practical applications H^+ nuclei are measured because of their sensitivity and their density in organic matter. The temporal behavior of the relaxation however strongly depends on how the nucleus is held together chemically.

2.3. Relaxation Times

The magnetic momentum \mathbf{M} will result from a superposition of the momentum of all nuclei of the corresponding volume. During relaxation the vector \mathbf{M} of the magnetic momentum can be decomposed into components in the direction of the external constant field (z) and in those perpendicular (x,y). This is illustrated in figure 2a, which shows the vectorial components of \mathbf{M} . After relaxation into the equilibrium, the \mathbf{M}_{xy} components of \mathbf{M} will be decreased to zero and \mathbf{M} will be equal to \mathbf{M}_z again. The temporal behavior of \mathbf{M}_z and of \mathbf{M}_{xy} components are described by two time constants T_1 and T_2 , that are also shown in figure 2.

T_1 describes the relaxation process in z direction (longitudinal relaxation) and the growth of the \mathbf{M}_z component by exchange of energy with the environment, whereas T_2 stands for the decrease of the \mathbf{M}_{xy} component (transversal relaxation). Both constants are only weakly correlated, since statistical phase shifting of single spins accelerate the reduction of the sum \mathbf{M}_{xy} .

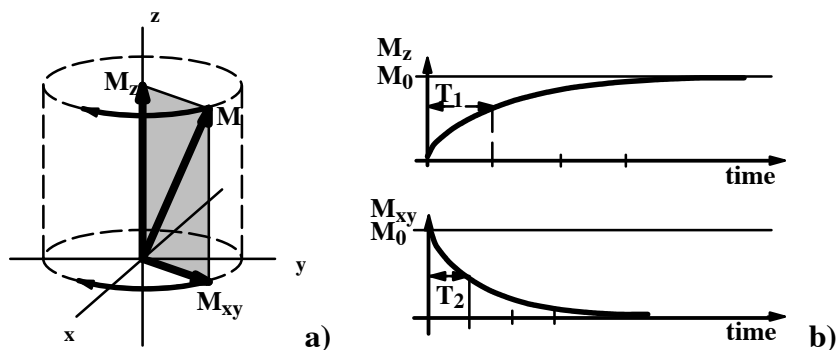


Figure 2. a) Magnetic Momentum \mathbf{M} and it's components
 b) Temporal relaxation behavior of the components of \mathbf{M}

Finally, it can be stated, that the echo measured depends on numerous parameters, as:

- spin density
- relaxation T_1
- relaxation T_2
- chemical shifts
- flux (blood)

The following paragraph briefly describes one of the pulse sequences of the stimulating HF-field to measure T_1 and to generate T_1 weighted images.

2.4. Measuring T_1 -Relaxation with Spin-Echo Sequences

In addition to saturation recovery and inversion recovery, the spin-echo sequence (see figure 3) is one of the three most important impulse sequences used for measuring the parameters stated above. In order to measure a signal which depends mainly on T_1 the M_z component has to be tipped into the xy -plane, where the signal can be detected. This is performed by a first 90° pulse. The coherence of the single spins however will rapidly get lost and the resulting response will decrease with time. This is shown in figure 4. In order to create an echo a second 180° pulse will invert the phase drifts and will generate coherence again for a short time interval. The maximum response resulting from this can be measured at the echo-time T_e .

After this second 180° pulse the relaxation process will turn the magnetic momentum again into its equilibrium. If we repeat the pulse sequence described above with a time rate T_R that is much shorter than T_1 the actual strength of the measured response will strongly depend on the T_1 of the respective nucleus. If, however, T_R is longer than T_1 the resulting echo will mainly depend on T_2 and on the density of the spins.

Choosing respectively short repetition times, a value that represents the T_1 and characterizes the nucleus will be received for each volume element .

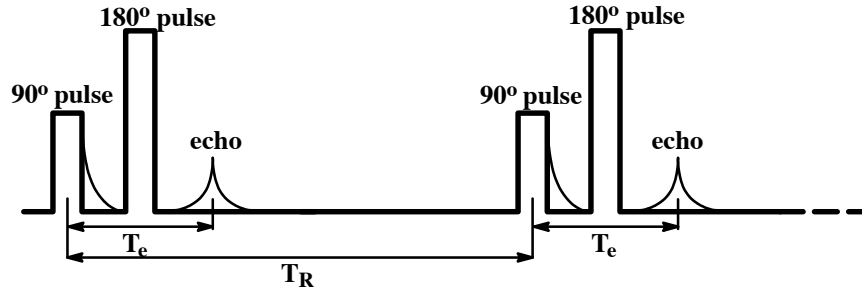


Figure 3. Spin-Echo sequences characterized by echo time T_e and pulse repetition time T_R

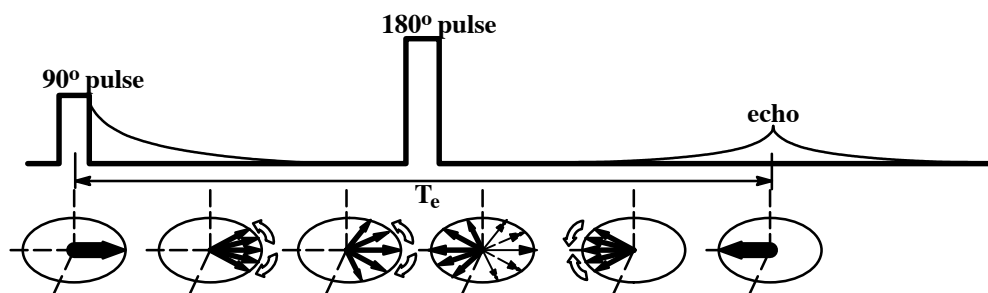


Figure 4. Temporal loss of phase coherence in the M_{xy} component of the Momentum

Finally, the question arises how to code the spatial position of the volume elements in 3D and how to look inside the volume. If we look back to the Lamor equation (eq. 1) we remember that the resonance frequency depends on the strength of the magnetic field. Using this relationship additional gradient magnetic fields in x , y and z direction can be superimposed to code the spatial position in terms of different Lamor frequencies for one type of

nucleus. The 3D volumetric image itself can then be obtained by methods such as an inverse 3D Fourier transform of the data set measured. This will not be described here in detail but can be found in [15] or [20].

3. Clustering and Classification with Topological Mapping Networks of Kohonen

3.1. General Remarks

After being introduced to the physics of MR–images the question arises how to set up a method for the automatic recognition, classification and visualization of the data. In statistical data analysis we may find numerous methods to perform these tasks[4].

In general, a robust classification pipeline can be defined as follows:

It consists of three different tasks to be solved separately

- I) feature extraction
- II) cluster analysis
- III) supervised classification based on interactive selection of training patterns

The goal of a feature extractor is to find a limited set of invariant descriptors that characterizes the data in a proper way. In this case the standard methods of texture analysis could be used as in [9]. A further way to extend the features taken from texture analysis is to inject a contrast medium and to record a second scene. Cluster analysis should give an indication about the statistical distribution of the feature vectors. Since it will be generally multidimensional, we will face the problem of visualizing its topological structure which is of importance for the selection of training areas for a supervised classification method.

Artificial neural networks have proved to be an interesting alternative to standard methods and several application studies have shown their advantages [23].

In the following section we propose a neural network which is capable of solving these tasks in a unique paradigm and allows subspace mapping and visualization of the multidimensional texture feature space for the interactive selection of training patterns.

3.2. Topology and Training Rules of Kohonen Mapping

The Kohonen Map, introduced in [11] or [12], is a self–organizing network which is basically trained without supervision. Its objective is the organization of the input patterns to a topological structure represented by its neurons, where the relations between different patterns are preserved.

The Kohonen map is a two–layered network. The first layer of neurons can be considered as a group of sensors picking up the data. It is entirely connected to a second, two–dimensional layer: the competitive layer. Figure 5 shows the topology of the network. The weights associated with the connections are adjusted during training and only one single neuron in the competitive layer can be active at a time. This neuron represents the cluster which the data set belongs to. Due to the training rules explained below, the spatial distance of two neurons reacting on different input patterns is a measure for the similarity of the two patterns.

The training of the network is carried out by presenting data vectors \mathbf{x} to the input layer of the network whose connection weight vectors \mathbf{m}_i of all competitive neurons i are chosen by random values. If N is the dimension of the data, we chose N input neurons and define an Euclidean distance d_i between \mathbf{x} and \mathbf{m}_i with

$$d_i = \|\mathbf{x} - \mathbf{m}_i\| = \sqrt{\sum_{j=1}^N (x_j - m_{ij})^2} \quad (2)$$

The neuron c with the minimum distance is then activated, where

$$d_c = \min_i(d_i) \quad (3)$$

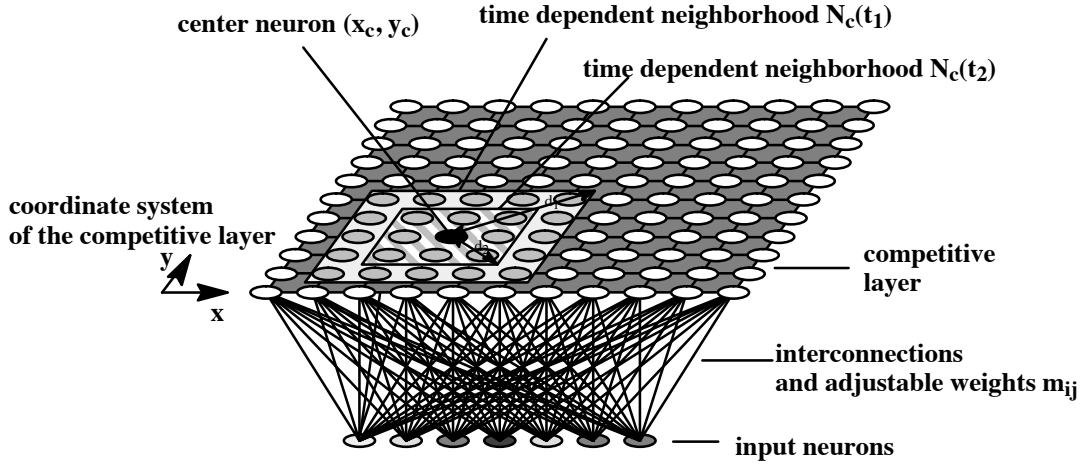


Figure 5. Topology of the Kohonen map and the time dependent neighborhood $N_c(t)$ of a neuron c

The updating of the weights m_{ij} associated to the neurons is only performed within a proximity ($i \in N_c(t)$) of c . This proximity $N_c(t)$ is reduced with training time t . The updating follows equation 4, where $a(t)$ represents a time-dependent learning rate:

$$m_{ij}^{(t+1)} = m_{ij}^{(t)} + \Delta m_{ij}^{(t)} \quad (4)$$

$$\Delta m_{ij}^{(t)} = \begin{cases} \alpha(t)(x_j - m_{ij}^{(t)}), & \text{if neuron } i \in N_c(t) \\ 0, & \text{otherwise} \end{cases} \quad (5)$$

$$\alpha(t) = \alpha_0 \left(1 - \frac{t}{T}\right), \quad t \in [0, \dots, T] \quad (6)$$

The time-dependent neighborhood, which is also illustrated in figure 5, is updated according to:

$$d(t) = d_0 \left(1 - \frac{t}{T}\right), \quad t \in [0, \dots, T] \quad (7)$$

Thus, the network performs two features during the training that are strongly related to our problem:

- I. A separation, i.e. cluster analysis of the presented data by mean vectors m_i that are associated as weights to the neurons.
- II. A topological ordering of the competitive neurons in such a way that neighboring neurons in the layer represent similar clusters in multidimensional space and thus a dimensionality reduction.

This can also be interpreted as a nonlinear, topology preserving, associative mapping process.

Generally, the Kohonen Map refers to the classical iterative optimization techniques, well-known from C-means clustering [2].

3.3. Visualizing Neighbored Clusters in a High Dimensional Texture Space

The previous section we have shown that the standard Kohonen Map can be used to reduce the dimensionality of data sets used for training. To do so, the number of input neurons has to be equal to the dimension of the input data, where each data vector is presented simultaneously to the net. For the neurons in the competitive layer are ordered topologically, i.e. neighboring neurons react to data vectors similar in the input space, the mapping can be interpreted as a reduction of any N -dimensional space into 2 dimensions preserving the topology of the data

as much as possible. The resolution of this discrete 2D space is given by the number of competitive neurons, i.e. clusters.

The visualization of cluster connectivity in high-dimensional spaces is, however, very important for the interactive process of selecting training areas for a supervised classification step. In order to map this onto color attributes, an easy-to-use and efficient scheme had been developed by Gross and Seibert (see [6] and [7]). We have extended this method by introducing a texture-based topology with a 3D competitive layer.

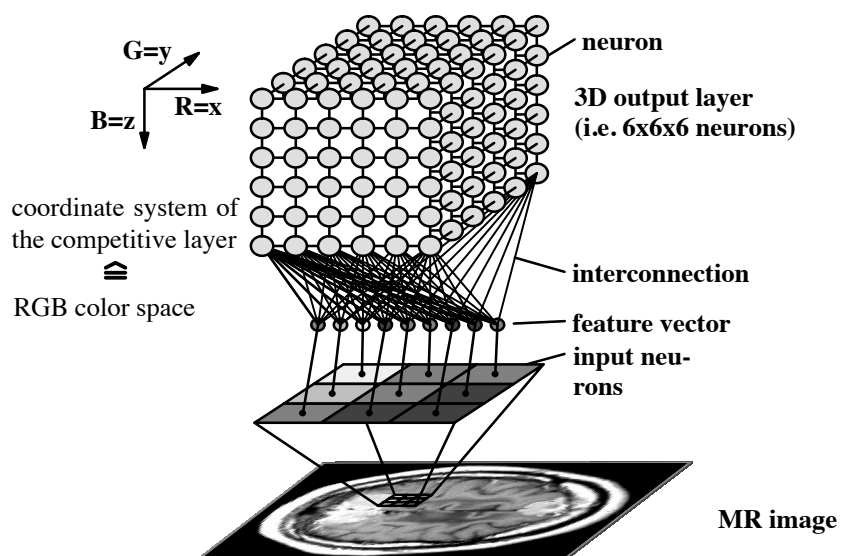


Figure 6. 3D Extension of the Kohonen – map with a 2D-3x3 input layer

Referencing the axes of the cube with the primaries R, G and B each neuron of the competitive layer represents a discrete entity in RGB space, i.e. it corresponds to a color triplet. The time-dependent neighborhood can easily be extended to 3D.

Since the network now arranges the neurons topologically during random training on the image, neighboring neurons with similar colors react to texture features neighbored in multidimensional space. Thus, the similarity of the color provided by the reacting neuron refers to a neighborhood in N-dimensional space.

Since visual data analysis is a perceptual task of human vision [7] and the RGB presentation is not a perceptual color space, post processing transformations can improve the result, for instance by referencing in CIE-Lab or CIE-Luv or others.

3.4. Supervised Classification with Learning Vector Quantization

So far, the Kohonen map has only been used for clustering, topological organization and for subspace mapping. For supervised classification however, each neuron – and also each cluster centroid – has to be assigned to a certain class depending on the definition of the user. This can be done by interactive selection of training areas and by a majority voting of each neuron stimulated by the training set. After this, each neuron has an associated class and the network is able to classify. However during the organization process the goal was to find a limited set of centroids representing the data in a C-means sense. As a result the centroids represent the variety of feature vectors in an optimal way leading to a minimum of the error function, which can be easily calculated by the Eukildean distance between all feature vectors and their nearest codebook vector. The self-organization does not yield to optimal decision boundaries, since class assignments were not taken into account. For this reason, the network can be trained again in order to move corresponding centroids towards the Bayes decision boundary and to improve the classification result.

This postprocessing is known as learning vector quantization (LVQ) [11] and can be described as follows:

For a given input pattern \mathbf{x} let \mathbf{m}_i and \mathbf{m}_j be the closest centroids to \mathbf{x} . We modify these mean vectors according to

$$\begin{aligned} \mathbf{m}_i(t+1) &= \mathbf{m}_i(t) - \alpha \cdot [\mathbf{x}(t) - \mathbf{m}_i(t)] & \text{if } & \mathbf{m}_i \text{ and } \mathbf{m}_j \text{ are the two closest weight vectors} \\ & & & \text{to the input vector } \mathbf{x}, \\ \mathbf{m}_j(t+1) &= \mathbf{m}_j(t) + \alpha \cdot [\mathbf{x}(t) - \mathbf{m}_j(t)] & & \mathbf{x} \text{ and } \mathbf{m}_j \text{ belong to the same class,} \\ & & & \mathbf{x} \text{ and } \mathbf{m}_i \text{ belong to different classes and} \\ & & & \mathbf{x} \text{ is falling into the window} \end{aligned}$$

$$\begin{aligned} \mathbf{m}_k(t+1) &= \mathbf{m}_k(t) + \varepsilon \cdot \alpha \cdot [\mathbf{x}(t) - \mathbf{m}_k(t)] & \text{if } & \mathbf{x}, \mathbf{m}_i \text{ and } \mathbf{m}_j \text{ belong to the same class} \\ & & & (k \in \{i, j\}) \\ & & & \text{where } \varepsilon \text{ is a small constant} \end{aligned}$$

This window is defined as a symmetric area around the midplane of \mathbf{m}_i and \mathbf{m}_j . Then \mathbf{x} falls into the window if

$$\min\left(\frac{d_i}{d_j}, \frac{d_j}{d_i}\right) > s \quad (8)$$

$$s = \frac{1-w}{1+w} \quad (9)$$

Where d_i and d_j are the two distances of \mathbf{x} to \mathbf{m}_i and \mathbf{m}_j . The threshold s is calculated according to eq. 9 and the relative window size w is chosen to app. 20%.

4. Application

4.1. General Remarks

In medical treatment of cancer patients magnetic resonance imaging systems are of increasing importance in diagnosis, therapy planning and supervision. In particular when facing brain tumors exact knowledge about the localization and extension of the tumor in the skull is essential for surgical procedures as well as for radiotherapy. In surgery, on the one hand, the tumor has to be removed entirely without damaging other important parts of the brain, nerves or veins. Radiotherapy, on the other hand, which focuses high energy radiation into the center of the tumor has to be parametrized in a way that the damage of the surrounding tissue is minimized. Finally, a long term supervision of the tumor's development has to follow for the patient's safety.

The standard process of human interpretation and diagnosis of these images is based on the expert knowledge of the physician and on the significant differences of tissue textures in the images. Usually, affected areas are indicated by interactive editing of the image. For these reasons, an automatic procedure as a support for the interpretation, classification and fast 3D-reconstruction of the initial images would be very helpful to the physician.

The following section describes an application of the methods introduced for the recognition and interpretation of brain tumors from MR images. We illustrate how the clustering and visualization algorithm works and show that LVQ training can successfully separate tissue types. Finally, a generalization to unknown images is provided. For reasons of performance in clinical procedures, we use a modified marching cubes algorithm for fast 3D-reconstruction.

4.2. Raw Image Data Used

The images shown in figure 7 present a typical set of T_1 -weighted MR image slices of a brain cancer patient affected by two meningioma. They were recorded with a spin-echo sequence of $T_R = 600$ ms and $T_e = 15$ ms. The spatial resolution is approx. 1 mm in the image plane and the signal is coded with 12 bits. Figure 8 shows the same image after applying a contrast medium (Gadolinium) to the patient, where the echo of the tumor appears much brighter. This image set illustrates that a standard linear separation of the grey values as proposed in [19] will never lead to reliable segmentation since the fat tissue surrounding the skull renders the same grey value. Bones cannot be seen in the images because of their low resonance signal.

Figure 7. *T₁-weighted MR image slices (precontrasted)*

Figure 8. *T₁-weighted MR image slices (postcontrasted)*

4.3. Clustering and Visualizing the Texture Features

As introduced in chapter 3, we applied our artificial neural network of size 6x6x6 neurons on the two image data sets (figures 7 and 8) and trained it on one slice by selecting randomly center pixels and a 3x3 environment in the pre- and postcontrasted images. Thus, we defined a raw texture description for further analysis, using 18 grey-values, since we accumulate for one pixel position greyvalues of both images in one feature vector. Figure 11 shows the result of the cluster analysis and dimensionality reduction from 18 to 3, namely RGB. The similarity of the colors stands for neighbored neurons responding to a similarity of the local texture elements. We see that

the larger tumor appears yellow and can be separated from the smaller one (blue) and from other tissue types in all slices of the data set. The network was trained for 20000 cycles.

4.4. Supervised Classification

Using the clustering results as a base, it is possible to define and evaluate polygonal training areas for a supervised method, as shown in figure 10. For each of the 7 anatomical classes defined, pixels within the polygons representing that class were used to train the network with LVQ postprocessing in 50000 cycles. The result of the supervised method for one selected slice is shown in Figure 12.

Although the clustering results indicated the possibility of separating the tumors from other tissue types, some errors still remain stemming either from inadequate training areas or from local minima. This result can be improved by interactive masking of the neurons in the Kohonen cube, as shown in figure 13 (upper left). Interactive masking optimizes the class assignments of selected neurons, which leads to an optimizing shift of the decision boundaries. The improved result in figure 13 (upper right) is based on this additional information, that was not included in the training areas.

The optimized classifier was applied on the entire image data set (see figure 13 lower) and serves as an input for 3D-reconstruction techniques.

4.5. Generalization

The reliability of a classifier is always evaluated by the capability to generalize the classification to data sets it was not trained on. With the requirement of similar parameters used for image scanning, physically corresponding images can be generated as in figure 9.

a) b)

Figure 9. Raw images for testing the generalization capability (T_1 -weighted image)
a) precontrasted image
b) postcontrasted image

In this case the interpretation is much more difficult for the physician. The contrast medium increases the signal behind the left eye of the patient as well as in the rear right part of the cortex. A determination of the tumor boundaries is very difficult due to the fact that the edge between the healthy tissue and the pathological tissue is not well defined. Applying the Kohonen map (trained on image data shown in figure 7) for clustering we achieve a result as in figure 14 (left), that reveals the characteristics of the pathological tissue. As the image contains the same

tumor type (meningioma) the network indicates these regions with yellow colors. Furthermore, the classified image is shown in figure 14 (right).

The results of this section are very promising, because the network trained on only one pathological data set is able to generalize the clustering and classification results to other comparable data sets. Using a statistically representative data base of brain cancer victims, we could optimize one large scale network and apply it to further new data stemming from everyday clinical requests for diagnosis.

4.6. Surface Reconstruction

The classified image slices from figure 13 can serve as an input for any kind of surface reconstruction or volume rendering method. For surgery and radiotherapy we need a fast and reliable method to achieve a 3D shape from our sparse data slices more than photorealistic ray traced images from slices of extreme density.

One problem arises when applying algorithms like a "marching cubes" on a classified data set with a low number of slices: We have to solve the task of interpolating "in-between" i.e. classified image slices instead of simple grey value slices.

To solve this problem, we use a modified weighted interpolation scheme, which is based on a distance weighted maximum decision for the class assignment of the respective voxel to be interpolated. The interpolation takes into account both the distances and the frequency of the labels on the vertices for the derivation of the label of any interpolated voxel coordinate.

The generation of surface polygons can be performed by a marching cubes algorithm [16] acting on the classified and interpolated image slices. With a simple modification, the two possible states of a vertex, namely "inside" or "outside" of the surface can be obtained considering the actual classes to be reconstructed, as for instance "tumor". According to the combination of "inside" and "outside" states in one cube consisting of 8 vertices, we built up a look-up table of precalculated triangles.

To provide the surface normal for the shading, we calculated standard surface normals out of the triangle geometry and stored them into the look-up table. This accelerates the rendering process. However we will only get a limited set of different triangles and normals which leads to a more "boxlike" appearance of the image. Another way would be to calculate the normals out of the grey level gradients from the raw image. But this gives rise to artefacts stemming from the difference between the density or response of a voxel and its class assignment that only corresponds, if linear separation methods are applied.

With the method explained above images can be achieved, giving a detailed impression of the tumor's volume. For therapy planning it is necessary to compute the volume coordinates of the affected regions. Visual information of the localization of the tumor is given in figure 15 showing the tumor in a transparent skull from a top view.

5. Conclusion

The method introduced in this paper has shown how to successfully apply artificial neural networks for the clustering, visualization and classification of magnetic resonance image data sets in order to support physicians in diagnosis and therapy planning. The advantages of this method are the easy-to-use scheme in a unique mathematical model on the one hand and its flexibility and generalization capability on the other hand. Using the sub-space mapping of the network we can easily establish a visualization technique for high dimensional texture features. In particular the interaction between a supervisor and the network during the training phase allows an optimization of the classification performance. This method can serve as a high quality and efficient preprocessor for any kind of volumetric renderer in computer graphics.

Future research should be directed towards training the network with statistically representative brain cancer data bases and to apply it in clinical case studies.

6. Acknowledgement

This research was made possible by a financial support of the research division of the Deutsche Telekom as a part of the project KAMEDIN. Further thanks to the department of Biophysics and Medical Radiation Physics of the

German Cancer Research Center, which kindly provided the data sets. The authors would also like to thank F. Seibert for the implementation of the Kohonen mapping and their students H. Behrens and O. Staadt for the implementation of the surface reconstruction techniques.

7. References

1. Crawford, S.; Fall, T.: Projection Pursuit Techniques for Visualizing High-Dimensional Data Sets. In Nielson, Shriver (Edts.): Visualization in Scientific Computing. IEEE Computer Society Press, Los Alamitos, California, pp. 94 – 108, (1990)
2. Duda, R.; Hart, P.: Pattern Classification and Scene Analysis. New York: John Wiley and Sons, (1973)
3. Drebin, R.A., Carpenter, L., Hanrahan, P.: Volume Rendering, Computer Graphics, Vol.22, No.4, pp.51–58, (1988)
4. Fukunaga, K.: Introduction to statistical pattern recognition. 2nd. ed. , Academic Press, (1990)
5. Gonzales, R.G.: Digital Image Processing, New York: Addison – Wesley Publishing Company, (1992)
6. Gross, M., Seibert, F.: Neural network image analysis for environmental protection. In Grütznert (Edts.): Visualisierung von Umweltdaten 1991, GI, Berlin – Heidelberg – New York: Springer (1991)
7. Gross, M.: Physiological Aspects of Human Vision and Computer Graphics. EUROGRAPHICS '91 tutorial notes, Springer Publishing Company, to be published, (1992)
8. Hall, L.O. , Bensaid, A.M., Clarke, L.P., Velthuizen, R.P., Silbiger, M.S., Bezdek, J.C.: A Comparison of Neural Network and Fuzzy Clustering Techniques in Segmenting magnetic Resonance Images of the Brain, IEEE Transactions on Neural Networks, Vol. 3, No. 5, pp. 672–682, (1992)
9. Haralik, R.M.: Statistical and Structural Approaches to Texture. Proceedings of the IEEE, Vol.67, No.5, pp.786–804, (1979)
10. Höhne, K.H., Bomas, M., Pommert, A., Riemer, M., Schiers, C., Tiede, U., Wiebecke, G.: 3D Visualization of Tomographic Volume Data using the Generalized Voxel Model, The Visual Computer, Vol.6, No.1, pp.28–36, (1990)
11. Kohonen, T.: The Self-Organizing Map. Proceedings of the IEEE, Vol. 78, No. 9, pp. 1464–1480, (1990)
12. Kohonen, T.: Self-Organization and Associative Memory, Berlin – Heidelberg – New York: Springer (1984)
13. Levoy, M.: Display of Surfaces from Volume Data, IEEE CG&A, Vol. 8, No. 5, pp. 29–37, (1988)
14. Lippmann, R.: An Introduction to Computing with Neural Nets, IEEE ASSP Magazine, Vol. 3, No.4, pp. 4–22, (1987)
15. Lissner, J., Seiderer, M.: Klinische Kernspintomographie, Stuttgart, (1990)
16. Lorensen, W.E., Cline, H.E.: Marching cubes: A High Resolution 3D Surface Construction Algorithm, Computer Graphics, Vol.21, No.4, pp.163–169, (1987)
17. Meinzer, H.P., Meetz, K., Scheppelmann, D., Engelmann, U., Baur, H.J.: The Heidelberg Ray Tracing Model, IEEE CG&A, (1991)
18. Minsky, M., Papert, S.: Perceptrons. 2nd Edition, Cambridge, MA: MIT Press, (1986)
19. Ney, D.E., Fishman, E.K. Magid, D., Drebin, A.: Volumetric Rendering of Computed Tomography Data: Principles and Techniques, IEEE CG&A, Vol.10, No.3, pp.24–32, (1990)
20. Philips: Prinzipien der MR-Tomographie, Philips Medical Systems, Eindhoven
21. Rumelhart, D.; Hinton, E.; Williams, R.: Learning Internal Representations by Error Propagation. Parallel Distributed Processing: Explorations in the Microstructures of Cognition, Vol.1, Cambridge, MA: MIT Press, pp. 318–362, (1986)
22. Schad, L.R., Schmitt, H.P., Oberwittler, C., Lorenz, W.J.: Numerical grading of astrocytomas, Med.Inform., Vol.12, No.1, pp.11–22, (1987)
23. Stork, A., Groß, M., Saradeth, S.: The Analysis of Remotely Sensed Data with Neural Networks, Proceedings of European International Space Year's Conference, München, ESA Publication Division, pp.417–422, (1992)
24. Young, F.; Rheingans, P.: Visualizing Structure in High-Dimensional Multivariate Data, IBM Journal of Research and Development, Vol. 35, No. 1/2, pp. 97–107, (1991)

COLOR PICTURE SECTION

Figure 10. *Polygonal training areas for supervised classification*

Figure 11. *Cluster analysis, dimensionality reduction and visualization of local texture properties*

Figure 12. *Supervised classification of a selected slice*

Figure 13. *Upper left: Masked Kohonen cube*
Upper right: Optimized result
Lower: Classification of the data set

Figure 14. *Generalization with the Kohonen feature map*
left: Clustering result
right: Classification result

Figure 15. *Top view on reconstructed tumor and and on the skull*